




A study on the electrical and dielectric properties of $\text{SrGd}_x\text{Fe}_{12-x}\text{O}_{19}$ ($x = 0.00\text{--}0.05$) nanosized M-type hexagonal ferrites

B. Ünal¹, M. A. Almessiere^{2,3,*} , Y. Slimani³, A. Demir Korkmaz⁴, and A. Baykal⁵

¹Institute of Forensic Sciences and Legal Medicine, Istanbul University-Cerrahpasa, Buyukcekmece Campus, 34500 Buyukcekmece-Istanbul, Turkey

²Department of Physics, College of Science, Imam Abdulrahman Bin Faisal University, P.O. Box 1982, Dammam 31441 Saudi Arabia

³Department of Biophysics, Institute for Research and Medical Consultation (IRMC), Imam Abdulrahman Bin Faisal University, P.O. Box 1982, Dammam 31441 Saudi Arabia

⁴Department of Chemistry, Istanbul Medeniyet University, 34700 Uskudar-Istanbul, Turkey

⁵Department of Nanomedicine Research, Institute for Research and Medical Consultation (IRMC), Imam Abdulrahman Bin Faisal University, P.O. Box 1982, Dammam 31441, Saudi Arabia

Received: 6 May 2021

Accepted: 8 June 2021

Published online:
17 June 2021

© The Author(s), under exclusive licence to Springer Science+Business Media, LLC, part of Springer Nature 2021

ABSTRACT

Single-phase $\text{SrGd}_x\text{Fe}_{12-x}\text{O}_{19}$ ($x = 0.00\text{--}0.05$) nanosized M-type hexagonal ferrites (NHF) were prepared via citrate sol-gel route. The formation of Gd substituted Sr-hexaferrites has been confirmed by XRD, SEM, TEM and EDX for all substitutions. The X-ray powder patterns revealed the hexagonal crystal structure of all products. The electrical and dielectric properties of $\text{SrGd}_x\text{Fe}_{12-x}\text{O}_{19}$ NHFs were investigated extensively with an impedance spectroscopy up to 3.0 MHz from 20 to 120 °C. Both electrical and dielectric components including ac/dc conductivity, dielectric constant, dielectric loss and lossy tangent were evaluated for measurement temperatures up to 120 °C. It has been indicated that ac conductivity generally complies with power law rules, mainly dependent on Gd^{3+} -ion substitution ratios. The impedance analysis showed that due to the influence of various Gd^{3+} -ion substitution ratios in the NHFs, the conduction mechanisms can mainly be attributed to the grain-grain boundaries. The dielectric constant of $\text{SrGd}_x\text{Fe}_{12-x}\text{O}_{19}$ NHFs owns a normal dielectric distribution with the frequency, largely due to varying substitution ratios. In other words, the variation of Gd^{3+} -ion substitution can be used to modify the conduction mechanism of NHFs. Therefore, the observed change in dielectric properties as a function of frequency can be clarified on a phenomenological basis by Koop's model of the electrical conduction mechanism in most composite ferrites.

Address correspondence to E-mail: malmessiere@iau.edu.sa

1 Introduction

Hexagonal ferrites, also known as hexaferrites, are magnetic iron oxides with a hexagonal structure. They are formed by iron, oxygen and one or more other elements, which could be barium, strontium, cobalt or a combination of these [1]. There are structurally six types of hexaferrites (M, W, X, Y, Z, U) which have widespread applications as Permanent magnets, Electrical and microwave devices, Data storage and recording media, RAM (random access memory), microwave/EMI (electromagnetic interference) wave absorption, Magnetolectric (ME) and multiferroic (MF) applications, millimeter wave imaging, millimeter wave imaging, etc. [1]. Owing to their very unique physical properties (higher values of saturation magnetization, high electrical resistivity, high permittivity, high permeability, their tunable values of coercivity and low losses), M-type hexaferrites are suitable materials for permanent magnet applications and high-density recording media, etc. The room-temperature MF properties enable M-type hexaferrites to be employed in electromagnetic absorption in microwave region, high frequency applications, etc. [2–4]. The electrical properties of hexaferrites depend on both the type of hexaferrite and substituted element. All these properties can be tuned by the cationic replacements at $\text{Sr}^{2+}/\text{Ba}^{2+}$ and/or Fe^{3+} sites according to the requirements [5]. The rare earth ion (M^{3+}) substituted hexaferrites, due to their tuned dielectric properties, can be considered for specific device applications [6, 7]. We can encounter different studies regarding the substitution of hexaferrites by M^{3+} ions in the literature. For example, magnetic properties and hyperfine interactions (Mössbauer study) of gallium-doped M-type barium hexaferrites was studied by Trukhanov et al. [8]. The polarization origin and iron positions in indium-doped barium hexaferrites was examined in a study by Trukhanov et al. [9]. The effect of Nb substitution on magnetic properties of $\text{BaFe}_{12}\text{O}_{19}$ -nanosized M-type hexagonal ferrites was studied by Almessiere et al. [10]. The effect of magnetic, non-magnetic and dielectric ions substitution on magnetic and microwave properties of $\text{BaFe}_{12}\text{O}_{19}$ was studied by Sozeri et al. [11]. Baykal et al. studied the effect Pb substitution on microwave properties of Ba- and Sr-hexaferrite nanoparticles as high-quality microwave absorbers [12]. The magnetic and dielectric properties of bicomponent ceramics $[(\text{BaFe}_{11.9}\text{Al}_{0.1}\text{O}_{19})_1-$

$_x - (\text{BaTiO}_3)_x]$ containing the M-type crystal structure hexaferrite was studied by Trukhanov et al. [13]. The recent antenna application of M-type hexaferrites was explored by Darwish et al. [14]. In another study, Nemreva et al. showed the presence of three oxidation states of manganese in the Ba-hexaferrite ($\text{BaFe}_{12-x}\text{Mn}_x\text{O}_{19}$) [15].

Apart from M-type hexaferrites, other types of hexaferrites have been also intensively investigated. For instance, Häßner et al. synthesized a new hexaferrite with the composition $(\text{Ba}, \text{Pb})(\text{Fe}, \text{Ti})_9\text{O}_{15}$ by lead (II) oxide flux, which led to the incorporation of Pb^{2+} into the structure on the barium position [16]. The product showed ferrimagnetic behaviour with a Curie temperature of $T_c = 309.3\text{ }^\circ\text{C}$ and a strong indication for a magnetic phase transformation to ferromagnetic state at high magnetic field strengths and at temperatures below $-123\text{ }^\circ\text{C}$ [16]. Nowadays, exchanged coupled hard (M-type hexaferrite)/soft (M-type hexaferrite) magnetic nanocomposites are promising a new field of application [17–19]. In addition to their magnetic behaviour, hexagonal ferrites also exhibit interesting dielectric properties. Due to their interesting dielectric properties, they find large scale applications from microwave to radio frequency devices. The electrical properties of hexaferrites are highly sensitive to the type and element of substitution. By adding different cations and varying cations distribution between interstitial sites, the dielectric properties of the hexaferrites can be engineered for specific device applications [7, 20]. The doping of lanthanide (Ln^{3+}) on strontium hexaferrite in very small amounts leads to significant improvements in their properties [21]. Furthermore, the Ln^{3+} dopant is not only useful for tuning the hexaferrites internal characteristics, but also can contribute to controlling the grain size at a higher temperature [22]. It has been reported [23] that the rare earth ions can modify the physical properties due to the larger ionic radius, which resides at B sites.

The aim of the current study is to prepare Gd^{3+} -substituted M-type Sr-nanosized M-type hexagonal ferrites with the sol-gel auto-combustion method and investigate their structural, electrical and dielectric properties in detail.

2 Experimental

For the citrate sol–gel synthesis of $\text{SrGd}_x\text{Fe}_{12-x}\text{O}_{10}$ ($x = 0.00\text{--}0.05$) NHFs, $\text{Fe}(\text{NO}_3)_3 \cdot 6\text{H}_2\text{O}$ (98%, Merck), $\text{Sr}(\text{NO}_3)_2$ (98%, Merck) and $\text{GdCl}_3 \cdot 6\text{H}_2\text{O}$ (97%, Merck) along with citric acid have been used. The certain amounts of metal nitrates and citric acid were dissolved in separate beakers containing 25 mL DI water under continuous stirring followed by combining both solutions to form the reaction mixture, whose pH was arranged to 7 by a concentrated ammonia solution. Afterwards, the final solution was heated up to 150 °C and then to 320 °C to have a viscous solution and finally a gel forming NHFs precursor. The solid product was obtained after being calcinated at 1100 °C for 6 h.

The structural, morphological analyses and conductivity and dielectric measurements were done by Rigaku Benchtop Miniflex X-ray diffractometer (Cu $K\alpha$ radiation), FEI Titan ST scanning electron microscope (SEM, with EDX), FEI, Morgagni 268 Transmission electron microscopy and Novo-control Alpha-N high-resolution dielectric–impedance analyzer, respectively.

3 Results and discussion

3.1 Microstructure and morphology

The structures of $\text{SrGd}_x\text{Fe}_{12-x}\text{O}_{19}$ ($x = 0.00\text{--}0.05$) NHFs were investigated by analysis of XRD powder patterns (Fig. 1). All patterns showed pure phase M-type Sr-hexaferrite crystal structure without occurrence of impurities. As it can be seen from Fig. 1, all peaks perfectly matched with the file PDF-33-1340 in ICDD, confirming the formation of the hexagonal crystal structure. The average crystallite size (D_{XRD}) was calculated from (114) diffraction peak by applying a well-known Scherrer's formula and found to be in the range of 34–50 nm. All structural parameters were given in Table 1.

Figure 2 exhibited the SEM images of $\text{SrGd}_x\text{Fe}_{12-x}\text{O}_{19}$ ($x = 0.00\text{--}0.05$) NHFs. All samples displayed highly agglomerated hexagonal platelet particles. These hexagonal platelets are nano-scale in thickness and micro-scale in diameter (the edge length in the range of 650–850 nm and the thickness of the platelet is about 35–60 nm). Moreover, the structure and morphology were confirmed via TEM

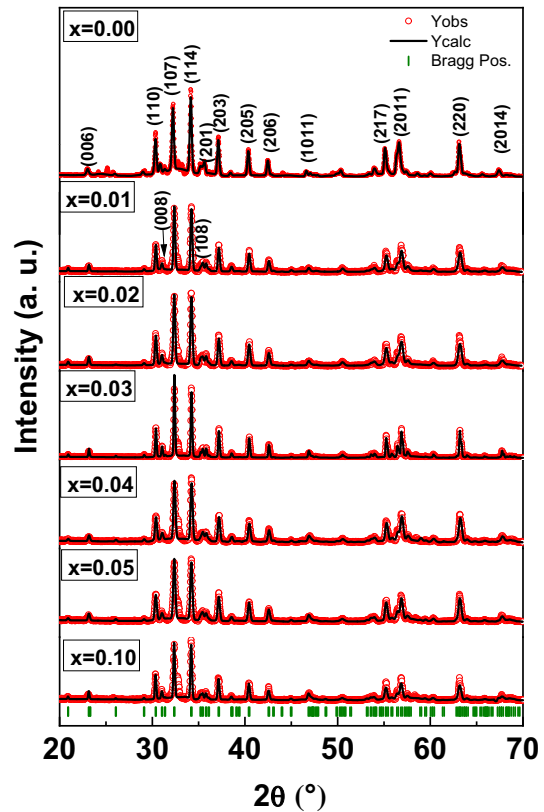


Fig. 1 XRD patterns of $\text{SrGd}_x\text{Fe}_{12-x}\text{O}_{19}$ ($x = 0.00\text{--}0.05$) NHFs

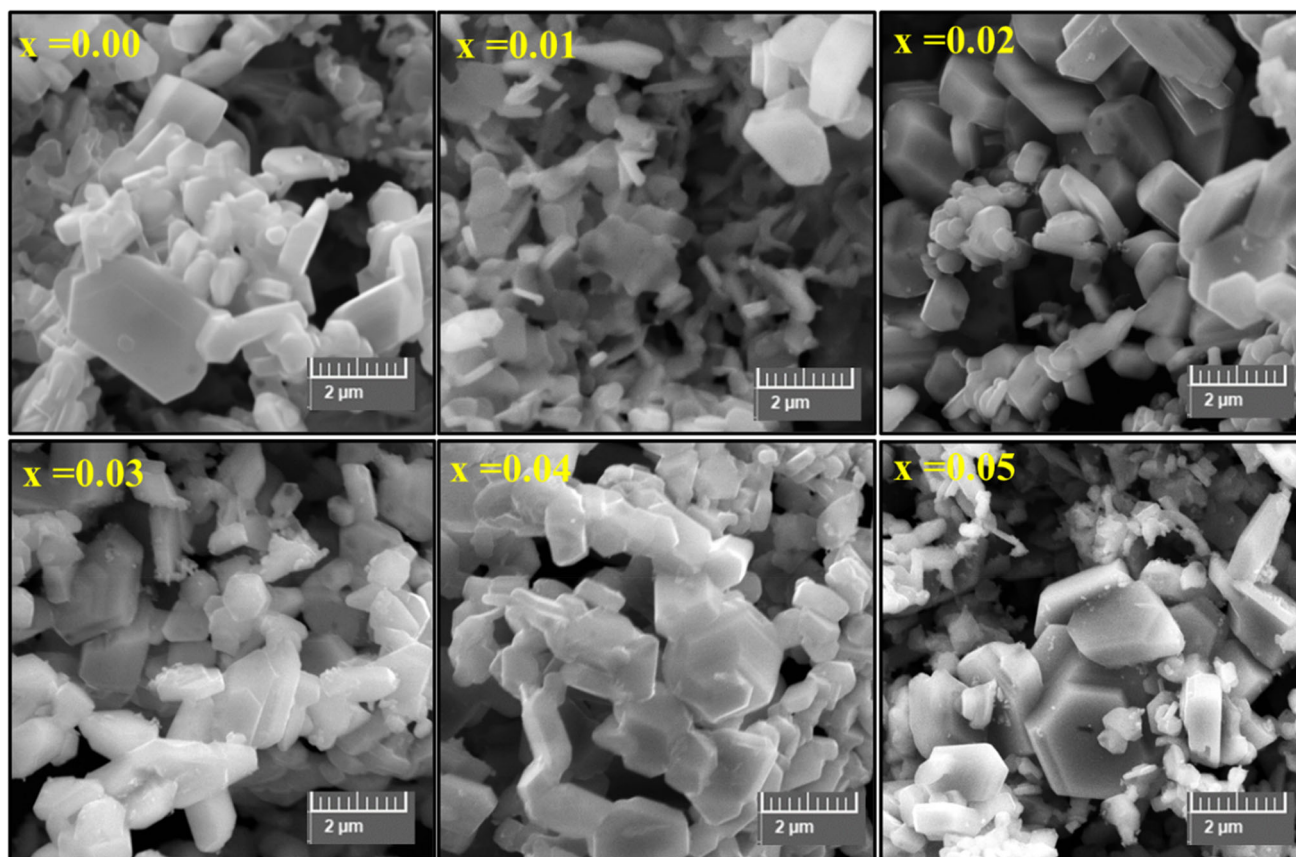
and SAED images as seen in Fig. 2. The composition content of $\text{SrGd}_x\text{Fe}_{12-x}\text{O}_{19}$ ($x = 0.03$) NHFs was analyzed through EDX and it was found that all elements matched well with their chemical formula as seen in Fig. 3.

3.2 Electrical and dielectric properties

The permittivity of a variety of ferrite materials is used to explain a variety of physical phenomena. Electronic polarization, atomic polarization, dipolar relaxation and ionic conduction are the main contributors to the permittivity of a dielectric material in general. In this study, dielectric losses are much more dominant in ionic conductivity at frequencies under the microwave region [24]. The electrical and dielectric properties of $\text{SrGd}_x\text{Fe}_{12-x}\text{O}_{19}$ NHFs were investigated by ac/dc conductivity, dielectric constant, dielectric loss and tangent loss as functions of variable frequency, temperature and substitution ratios. Thus, measurements of all dielectric parameters were carried out in the frequency range up to 3.0 MHz and at temperatures between 20 and 120 °C.

Table 1 Gd content, refined structural parameters for $\text{SrGd}_x\text{Fe}_{12-x}\text{O}_{10}$ ($0.00 \leq x \leq 0.05$) NHFs

x	$a = b$ (Å)	c (Å)	V (Å) ³	c/a	D_{XRD} (nm) \pm 0.13	χ^2 (chi^2)	R_{Bragg}
0.00	5.883 (8)	23.156 (6)	694.25	3.9357	35.89	2.46	2.40
0.01	5.884 (1)	23.049 (0)	691.10	3.9171	39.53	1.84	4.57
0.02	5.892 (2)	23.080 (1)	693.94	3.9170	38.25	1.82	9.10
0.03	5.893 (2)	23.085 (2)	694.32	3.9172	49.81	2.92	3.28
0.04	5.894 (5)	23.083 (4)	694.59	3.9164	33.83	2.16	5.63
0.05	5.894 (7)	23.086 (5)	694.73	3.9164	33.55	2.55	7.16

**Fig. 2** SEM images of $\text{SrGd}_x\text{Fe}_{12-x}\text{O}_{19}$ ($x = 0.00$ – 0.05) NHFs

3.3 AC conductivity

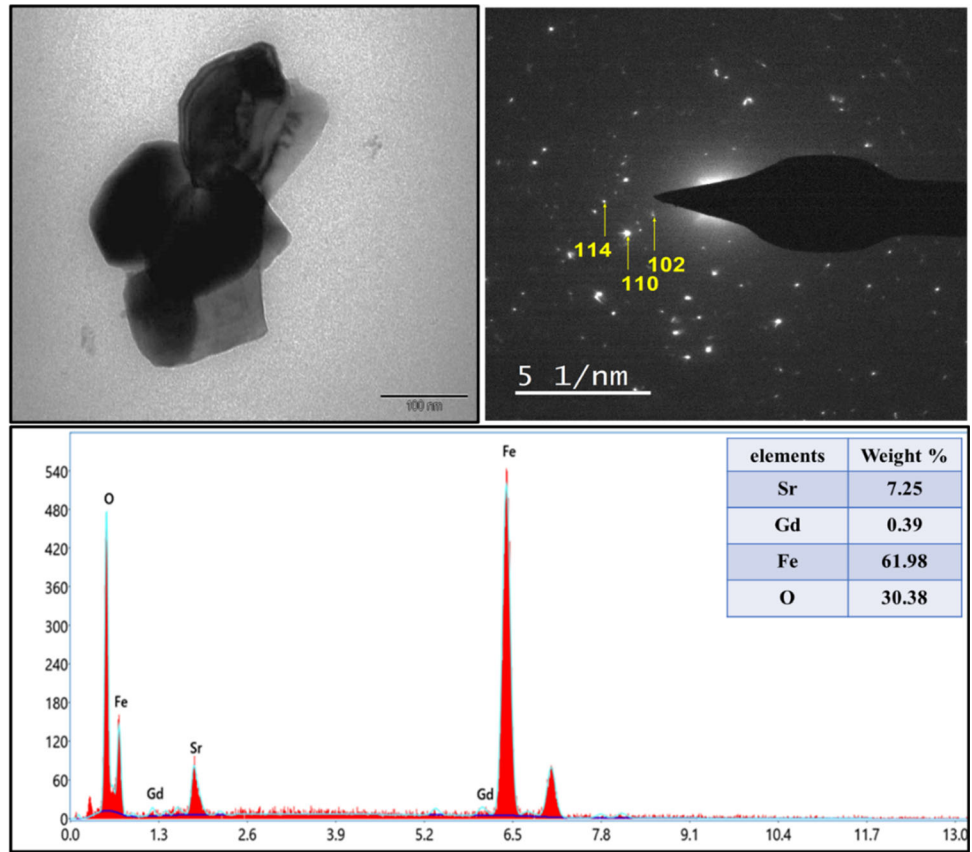
Both the conduction and mobility charging mechanisms can be elucidated by the ac conductivity study, which contributes to the performance of charge carriers under the influence of a variable electric field. The frequency dependent conductivity of almost all $\text{SrGd}_x\text{Fe}_{12-x}\text{O}_{19}$ NHFs based on the substitution ratios up to 0.05 can be evaluated by the following equation [25]:

$$\sigma_{\text{ac}}(\omega, T; x) = \omega \varepsilon_0 \varepsilon'(\omega, T; x) \tan \delta(\omega, T; x), \quad (1)$$

where ε' is the relative permittivity, ε_0 is the absolute permittivity, T is the measured temperature, ω is the angular frequency of the externally applied electric field and $\tan \delta$ is the tangent loss.

The 3D characterization of ac conductivity of $\text{SrGd}_x\text{Fe}_{12-x}\text{O}_{19}$ NHFs based on a variety of substitution ratios is shown in Fig. 4. Variations in the substitution ratios of Gd^{3+} ions, ranging from 0.00 to 0.05, have a great influence in modifying the conduction mechanism as functions of frequencies and temperatures. The general trend in ac conductivity variation shows the known conduction mechanism behaviour given in the above formula for all

Fig. 3 TEM micrograph, SAED pattern and EDX spectrum of $\text{SrGd}_x\text{Fe}_{12-x}\text{O}_{19}$ ($x = 0.03$) NHFs



$\text{SrGd}_x\text{Fe}_{12-x}\text{O}_{19}$ NHFs. The substitution of the Gd^{3+} ion into Sr NHFs were observed to get rid of the fluctuation and to improve the tendencies in conductivity across the temperature variation at higher frequencies. The conductivity increases with the rise in the temperatures at lower frequencies for all Sr NHFs while remaining almost unchanged in higher frequencies. Therefore, Gd^{3+} -ion substitution has a great effect on Sr-ferrite structures that causes that the conduction mechanism. It was observed that the conductivity obeyed the power law as follows [26]:

$$\sigma_{ac}(\omega, T; x) = \sigma_{dc}(T; x)\omega^{n(x)}, \quad (2)$$

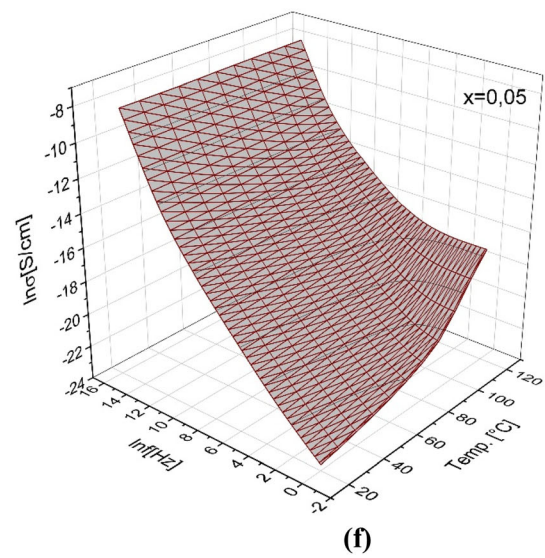
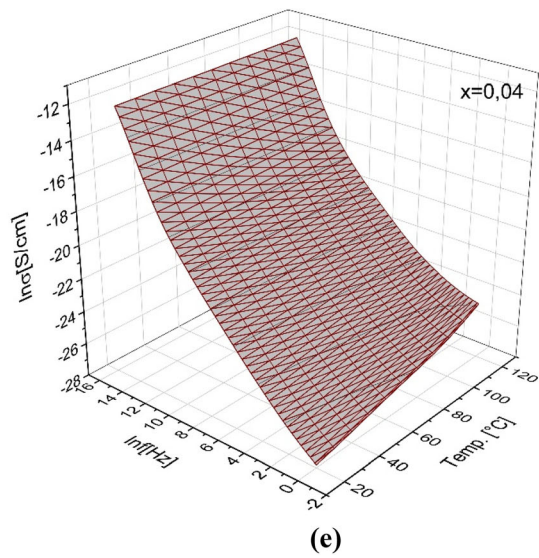
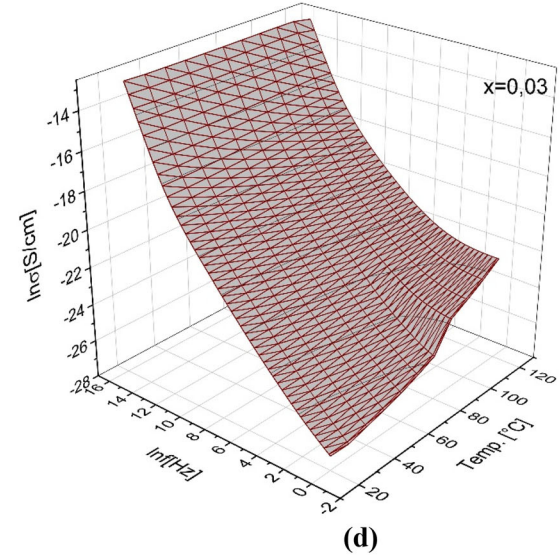
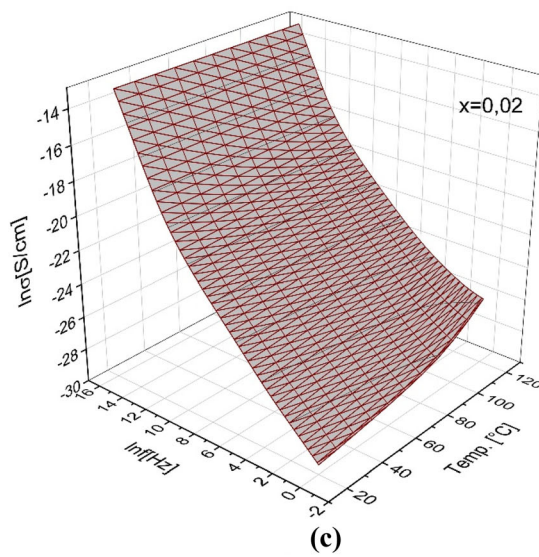
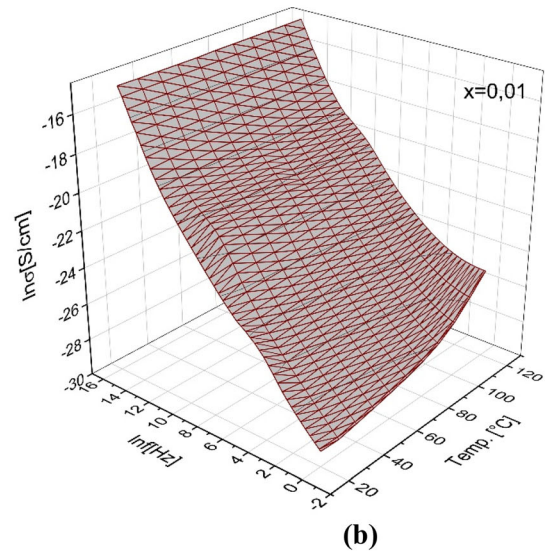
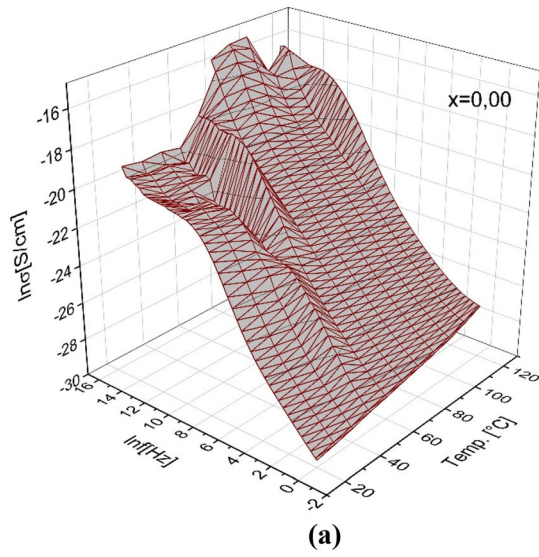
where $\sigma_{dc}(T)$ is the temperature-dependent dc conductivity and n is the power exponent. The conduction mechanisms for all Sr NHFs have a similar tendency to electric field variations with significant effects of substitution ratios.

3.4 Activation energy and DC conductivity

The 2D and 3D Arrhenius plots of dc conductivity for the $\text{SrGd}_x\text{Fe}_{12-x}\text{O}_{19}$ NHFs are depicted in Fig. 5a, b at temperatures up to 120 °C. In the 2D characteristic

representation, the dc conductivity is observed to increase with a rise in the substitution ratio and expresses a drop with the reciprocal temperatures. In general, the graphical Arrhenius representation shows that the two regions in activation energy occur along the increase of Gd^{3+} -ion substitution ratios in Sr NHFs. The similar trend is more clearly represented in the 3D Arrhenius plots in Fig. 5b.

Figure 5c clearly shows that the activation energy varies by two phenomenological tendencies with the Gd^{3+} ion substitution ratio of Sr NHFs as shown in Fig. 5c. Two regions were observed in the activation energy above and below 400 meV according to Gd^{3+} -ion substitution ratio up to 0.05. Linear tendencies in the activation energy were revealed in the low temperature region with values lower than 400 meV while fluctuated trends were measured in the high temperature region resulting in values over 400 meV up to 1459.1 meV. To put it more precisely, as the ratio of Gd^{3+} ions substituted into Sr NHFs increases, the activation energy on the high temperature side first increases rapidly from 440.8 to 970.1 meV, then decreases slowly to 568.7 meV and finally jumps abruptly to the maximum value of 1459.1 meV.



◀Fig. 4 3D representation of the ac conductivity of $\text{SrGd}_x\text{Fe}_{12-x}\text{O}_{19}$ ($0.00 \leq x \leq 0.05$) NHFs

Therefore, the relaxation process in the substituted Sr NHFs could be correlated with various defects in the conduction mechanism of charge carriers because of the Gd substitution ions. Consequently, the dc conductivity for each of the $\text{SrGd}_x\text{Fe}_{12-x}\text{O}_{19}$ NHFs can be expressed for the low and high T side as follows:

$$\sigma_{dc}(T; x) = \sigma_0(x) \exp\left(-\frac{E_a(x)}{k_B T}\right), \quad (3)$$

where $\sigma_0(x)$ is the conductivity at absolute temperature, k_B is the Boltzmann constant, x is the Gd^{3+} -ion substitution ratio, $E_a(x)$ is the activation energy in eV and $k_B T$ is the thermal energy. It can be clearly seen that the relaxation temperatures associated with the Gd^{3+} ion substitution ratio affect the activation energy. It should be noted that such a trend is very important in the electrical properties of the entire Sr NHFs. Therefore, the drift mobility of charged carriers also affects from the increase in the Gd^{3+} -ion substitution ratio. As seen clearly in the graph, the temperature increase in Sr NHFs shows the change in

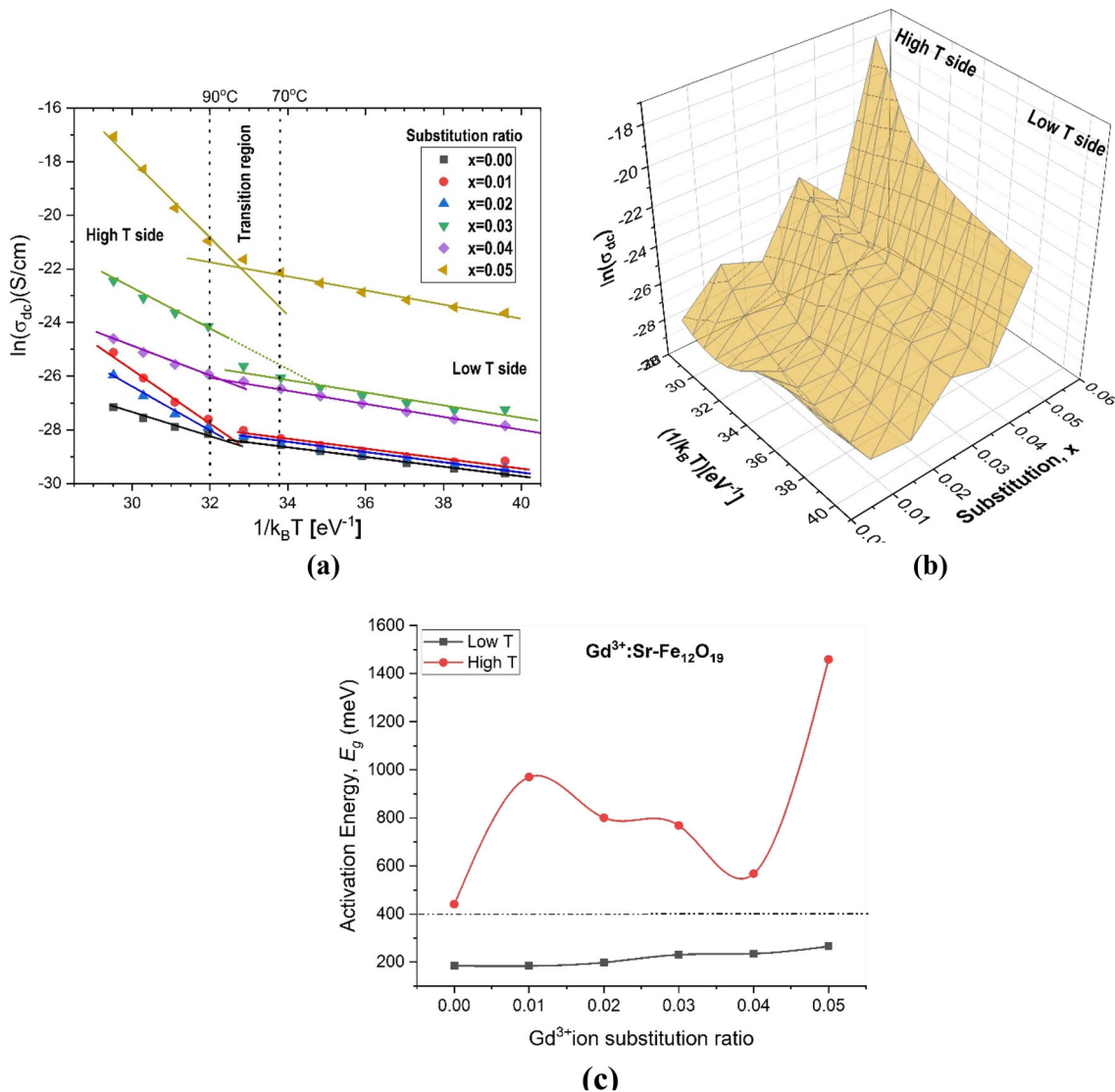


Fig. 5 a The 2D and b 3D Arrhenius representation of the dc conductivity and, c the activation energy of $\text{SrGd}_x\text{Fe}_{12-x}\text{O}_{19}$ ($x = 0.00-0.05$) NHFs

the thermal energy of the charge carriers and the change trend in the activation energy. Therefore, a suitable interpretation of this conduction mechanism can only be made by considering the structural effect of both the substituted and the host ion distributions in tetrahedral and octahedral regions. Due to the influence of various Gd^{3+} -ion substitution ratios in the Sr NHF, the conduction mechanisms can mainly be attributed to the grain-grain boundaries. Thus, the conduction performance in Gd^{3+} -ion-substituted Sr NHF can be explained significantly by the “Verwey Mechanism” [27].

3.5 Dielectric constant

The 3D characteristic representation of the dependence of the dielectric constant on both frequency and temperature for $\text{SrGd}_x\text{Fe}_{12-x}\text{O}_{19}$ NHF is shown in Fig. 6 for “ x ” substitution ratios between 0.00 and 0.05. The 3D representation offers a frequency of up to 3.0 MHz between 20 and 120 °C. It is clear that the dielectric constant of all Sr NHF decreases in different ways with the increasing frequency. However, their decay tendency as a function of frequency is almost different for all Sr NHF depending on the “ x ” and the temperature.

For $\text{SrGd}_x\text{Fe}_{12-x}\text{O}_{19}$ NHF (for $x = 0.0$), there is a sharp drop in temperature of about 60 °C for the central frequencies and then the drop becomes common across both the high frequency and low temperature values. Another sharp drop is observed at higher frequencies. When the measurement frequencies are reached above 1 MHz, it completely varies depending on the overall temperatures up to 120 °C. For the substituted Sr NHF, a sharp deterioration in the dielectric constant was noticed in the overall frequency range up to MHz levels for the entire Gd^{3+} -ion substitution rates. Although the temperature dependence appears insignificant at higher frequencies, it becomes more effective at lower frequencies. The effect of increasing temperature on the dielectric constant decreases with increasing frequency according to the observed results. It should be also noted that as the frequency increases, the dielectric constant decreases to a certain value, varying by the substitution ratios. At high frequencies, almost all composites show a sharp decline. It should be noted that the dielectric constant generally obeys the power exponent law as follows: $\varepsilon'(\omega, T; x) \propto \omega^{n(x)}$ where ω is the angular frequency of

the externally applied electric field. In addition, it is seen that the dielectric constant increases with increasing Gd^{3+} ion substitution ratio. So, it can be concluded that the characteristic variation of the dielectric constant in this study can be attributed to the occurrence of electrode interface polarization processes [28].

3.6 Dielectric loss

A 3D representation of the dielectric loss of $\text{SrGd}_x\text{Fe}_{12-x}\text{O}_{19}$ NHF with respect to their ratio of substitution is shown in Fig. 7. 3D characteristic graphs on the subject are represented as a function of temperature up to 120 °C and frequency up to 3.0 MHz. It has been observed that the dielectric loss for Sr NHF fluctuates throughout the frequency change for the entire temperature range up to 120 °C. For Sr NHF with a substitution ratio of $x = 0.01$, the dielectric loss increases with the temperature at low frequencies and remains constant during temperature change at higher frequencies but fluctuates with incremental frequencies. For all other substituted Sr NHF, the loss increases with the rise of temperature at low frequencies. The temperature dependence of the dielectric loss for all substitution ratios varies in a different way. Initially, it decreases with the frequency and then increases after reaching the minimum value. The structural basis of dielectric ferrite is considered to be composed of very fine conductive ferrite grains electrically insulated with fine-grained boundary layers. Such a variation in dielectric loss in rare earth ion substituted Sr NHF can be explained using Koop’s theory based on the Maxwell–Wagner model [29, 30].

3.7 Dissipation factor

The dissipation factor, in other words, the dielectric tangent loss (the ratio of the dielectric loss to the dielectric constant) of $\text{SrGd}_x\text{Fe}_{12-x}\text{O}_{19}$ ($x = 0.00$ – 0.05) NHF as a function of frequency at different temperatures is illustrated in Fig. 8. From the first plot of the figure ($x = 0.00$), the logarithmic tangent loss fluctuates considerably with the frequency and temperature, but less fluctuation in temperature change is observed for lower frequencies. For all substituted Sr NHF, the dissipation factor for the given Gd^{3+} -ion substitution ratios present certain trends depending on both temperature and frequency changes.

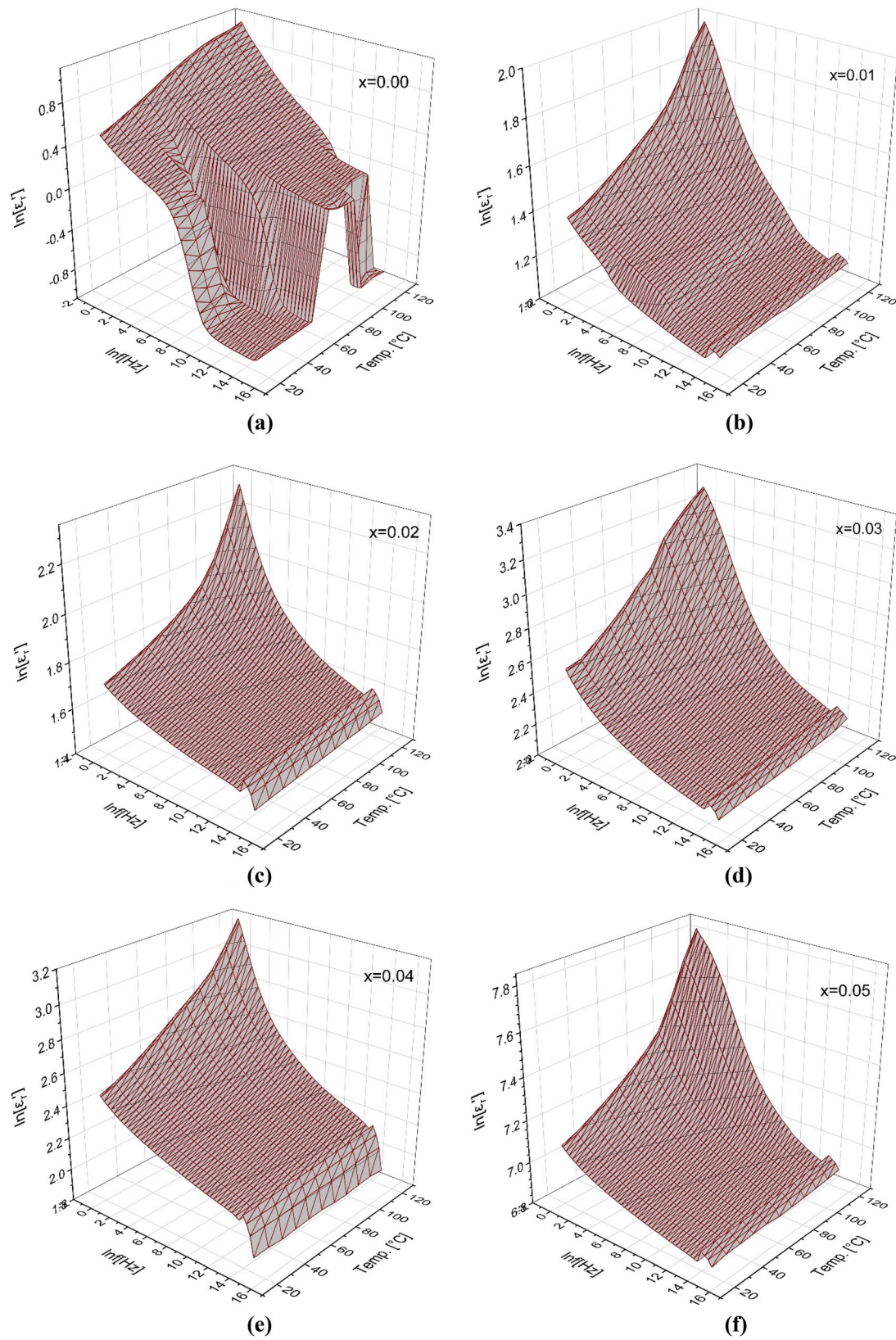


Fig. 6 3D representation of the dielectric constant of $\text{SrGd}_x\text{Fe}_{12-x}\text{O}_{19}$ ($x = 0.00\text{--}0.05$) NHFs

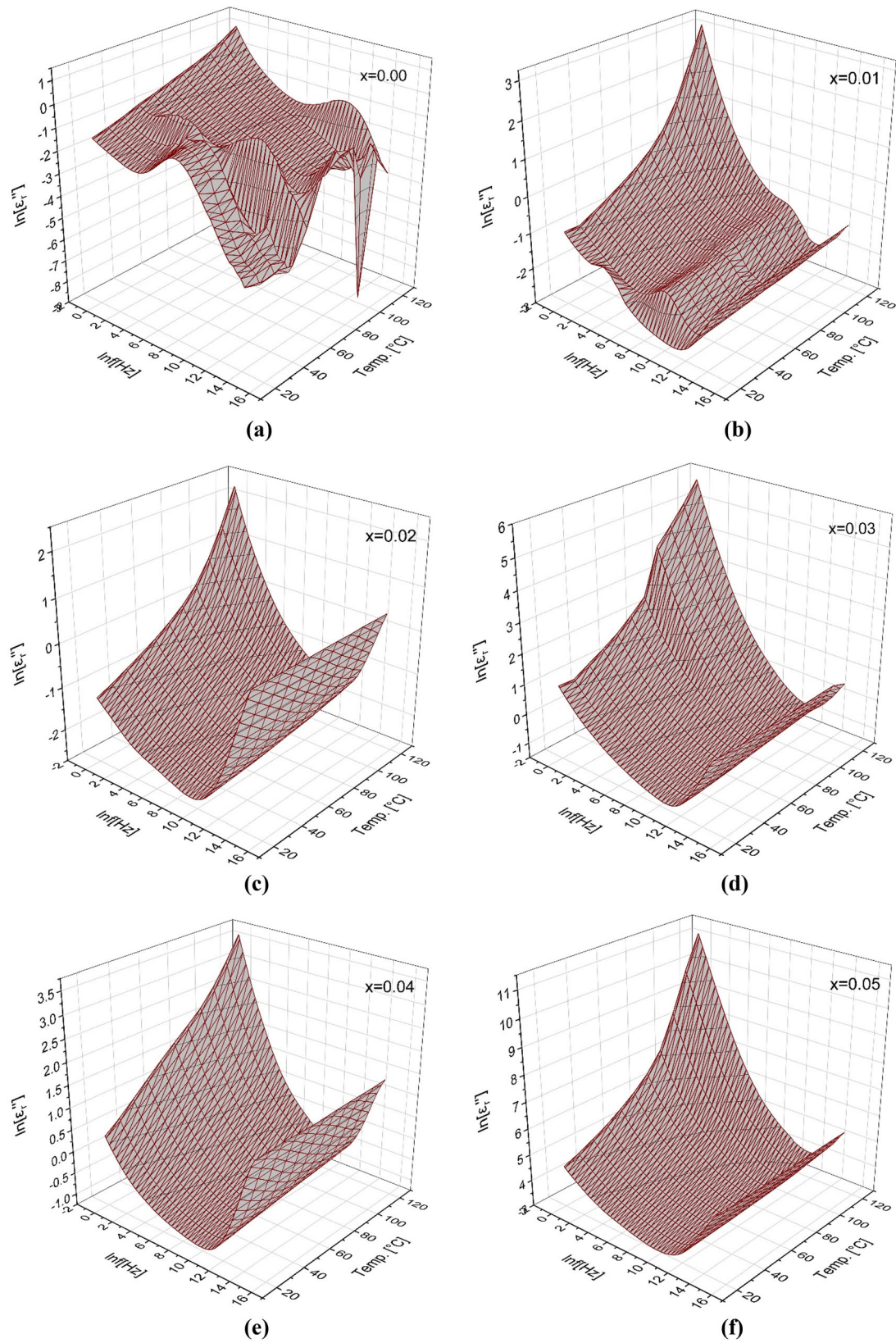


Fig. 7 3D representation of the dielectric loss of $\text{SrGd}_x\text{Fe}_{12-x}\text{O}_{19}$ ($x = 0.00\text{--}0.05$) NHFs

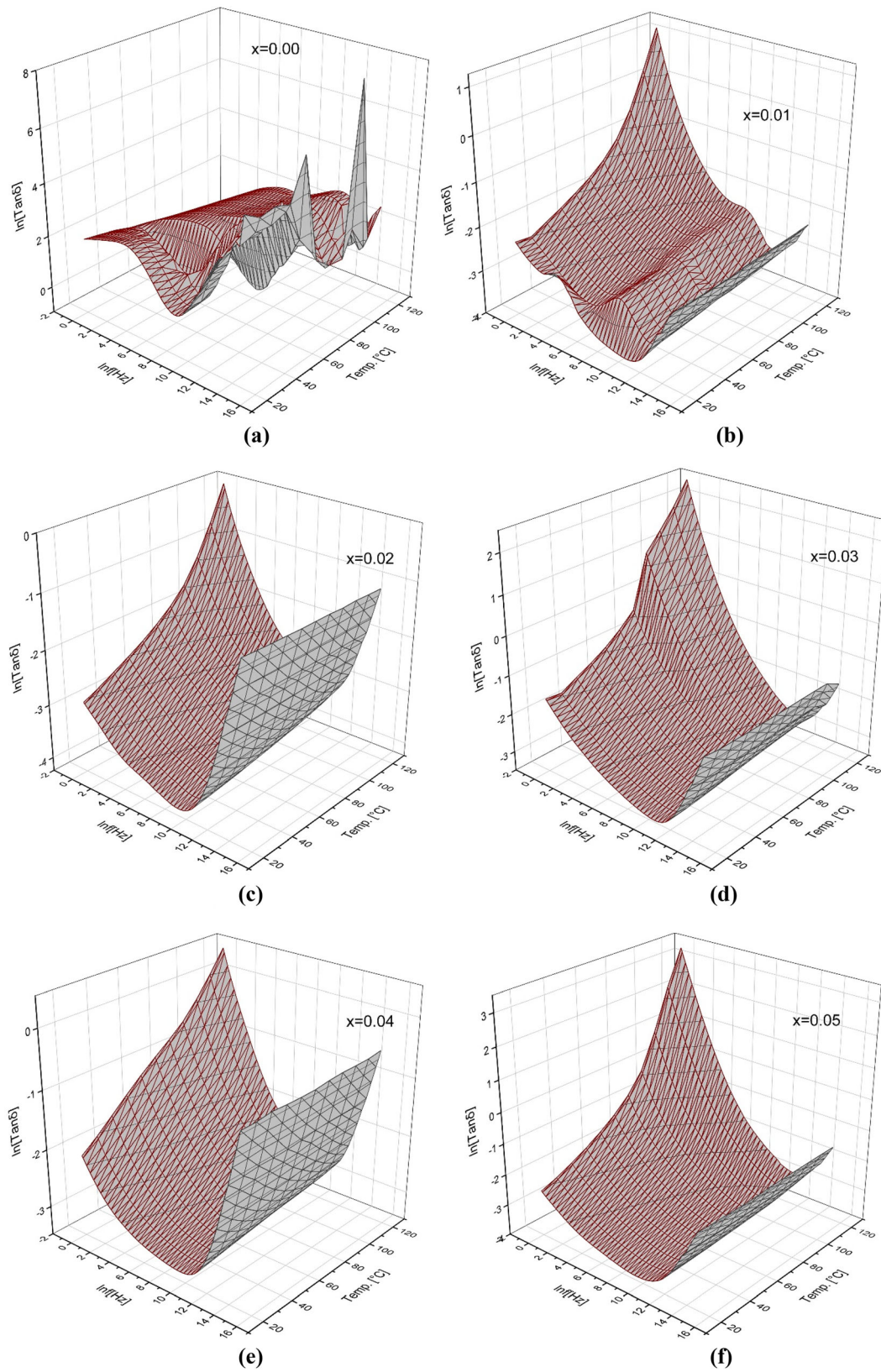


Fig. 8 3D representation of the dielectric tangent loss of $\text{SrGd}_x\text{Fe}_{12-x}\text{O}_{19}$ ($x = 0.00\text{--}0.05$) NHFs

Furthermore, the tangential loss, with increasing frequency for all temperature values, usually decreases sharply first, then reaches the minimum value and eventually starts to increase again. Especially for $x = 0.01$, this type of behaviour is slightly varied. Such trends in the tangential loss can be attributed to an effective dipole driven by the alternating electric field. It can be concluded that all trends in dielectric parameters may often differ for variable parameters such as frequency, temperature and substitution ratios. Therefore, by using both the temperature and frequency dependencies of the dissipation factor with the substitutional modification, NHFs can be utilized in technological applications, such as various gas, biosensors and some contrast agents for MRI devices.

4 Conclusion

Gd³⁺-substituted Sr-hexaferrites were fabricated by citrate sol-gel auto-combustion route. XRD, SEM, TEM and EDX results confirmed the formation of hexagonal crystal structure. The ac conductivity of Sr NHFs is observed to be strongly dependent on the substitution ratio. It can be also stated that conductivity variation generally obeys the power law rule of frequency despite some changes in the substitution ratios. Linear tendencies in activation energy were revealed in the low temperature region with values lower than 400 meV while fluctuated trends were measured in the high temperature region resulting in values over 400 meV up to 1459.1 meV. For all substituted Sr NHFs, the dissipation factor for the given Gd³⁺ ion substitution ratios present certain trends depending on both temperature and frequency changes. As a result, the trends in the electrical and dielectric parameters examined in this study can offer us many possibilities for certain technological applications such as various gas and biosensors, contrast agents for MRI devices and magnetic hyperthermia.

References

1. C. Robert, Pullar, hexagonal ferrites: a review of the synthesis, properties and applications of hexaferrite ceramics. *Prog. Mater. Sci.* **57**, 1191–1334 (2012)
2. S. Kumar, M. Kumar Manglam, S. Supriya, H. Kumar Satpal, R. Kumar Singh, M. Kar, Lattice strain mediated dielectric and magnetic properties in La doped barium hexaferrite. *J. Magn. Magn. Mater.* **473**, 312–319 (2019)
3. M.A. Almessiere, B. Unal, Y. Slimani, A. Demir Korkmaz, N.A. Algarou, A. Baykal, Electrical and dielectric properties of Nb³⁺ ions substituted Ba-hexaferrites. *Res. Phys.* **14**, 102468 (2019)
4. M. Amini, A. Gholizadeh, Shape control and associated magnetic and dielectric properties of MFe₁₂O₁₉ (M=Ba, Pb, Sr) hexaferrites. *J. Phys. Chem. Solids* **147**, 109660 (2020)
5. Y. Slimani, B. Unal, M.A. Almessiere, A. Demir Korkmaz, A. Baykal, Investigation of AC susceptibility, dielectric and electrical properties of Tb–Tm co-substituted M-type Sr hexaferrites. *Mat. Chem. Phys.* **260**, 124162 (2021)
6. H. Khanduri, M. Chandra Dimri, H. Kooskora, I. Heinmaa, G. Viola, H. Ning, M.J. Reece, J. Krustok, R. Stern, Structural, dielectric, magnetic, and nuclear magnetic resonance studies of multiferroic Y-type hexaferrites. *J. Appl. Phys.* **112**, 073903 (2012)
7. A. Zafar, S. Shahzada, A. Rahman, S. Anwar, M. Khan, A. Nisar, M. Ahmad, S. Karim, Electrical and magnetic properties of nano-sized Eu doped barium hexaferrites. *J. Alloys Compd.* **727**, 683–690 (2017)
8. A.V. Trukhanov, V.G. Kostishyn, L.V. Panina, S.H. Jabarov, V.V. Korovushkin, S.V. Trukhanov, E.L. Trukhanov, Magnetic properties and Mössbauer study of gallium doped M-type barium hexaferrites. *Ceram. Int.* **43**, 12822–12827 (2017)
9. S.V. Trukhanov, A.V. Trukhanov, V.A. Turchenko, An.V. Trukhanov, E.L. Trukhanova, D.I. Tishkevich, V.M. Ivanov, T.I. Zubar, M. Salem, V.G. Kostishyn, L.V. Panina, D.A. Vinnik, S.A. Gudkov, Polarization origin and iron positions in indium doped barium hexaferrites. *Ceram. Int.* **44**, 290–300 (2018)
10. M.A. Almessiere, Y. Slimani, N.A. Tashkandi, A. Baykal, M.F. Saraç, A.V. Trukhanov, İ Ercan, İ Belenli, The effect of Nb substitution on magnetic properties of BaFe₁₂O₁₉ nano-hexaferrites. *Ceram. Int.* **45**, 1691–1697 (2019)
11. H. Sözeri, Z. Mehmedi, H. Kavas, A. Baykal, Magnetic and microwave properties of BaFe₁₂O₁₉ substituted with magnetic, non-magnetic and dielectric ions. *Ceram. Int.* **41**, 9602–9609 (2015)
12. A. Baykal, İS. Ünver, U. Topal, H. Sözeri, Pb substituted Ba Sr-hexaferrite nanoparticles as high quality microwave absorbers. *Ceram. Int.* **43**(16), 14023–14030 (2017)
13. S.V. Trukhanov, A.V. Trukhanov, M.M. Salem, E.L. Trukhanova, L.V. Panina, V.G. Kostishyn, M.A. Darwish, T.I. Zubar, D.I. Tishkevich, V. Sivakov, D.A. Vinnik, S.A. Gudkova, C. Singh, Preparation and investigation of structure,

- magnetic and dielectric properties of $(\text{BaFe}_{11.9}\text{Al}_{0.1}\text{O}_{19})_{1-x}(\text{BaTiO}_3)_x$ bicomponent ceramics. *Ceram. Int.* **44**, 21295–21302 (2018)
14. M.A. Darwish, A.I. Afifi, A.S. Abd El-Hameed, H.F. Abosheishasha, A.M.A. Henaish, D. Salogub, A.T. Morchenko, V.G. Kostishyn, V.A. Turchenko, A.V. Trukhanov, Can hexaferrite composites be used as a new artificial material for antenna applications? *Ceram. Int.* **47**, 2615–2623 (2021)
 15. S. Nemrava, D.A. Vinnik, Z. Hu, M. Valldor, C.-Y. Kuo, D.A. Zhrebtsov, S.A. Gudkova, C.-T. Chen, L.H. Tjeng, R. Niewa, Three oxidation states of manganese in the barium hexaferrite $\text{BaFe}_{12-x}\text{Mn}_x\text{O}_{19}$. *Inorg. Chem.* **56**, 3861–3866 (2017)
 16. M. Häßner, D.A. Vinnik, R. Niewa, Structure and magnetic properties of a new hexaferrite $(\text{Ba}, \text{Pb})(\text{Fe}, \text{Ti})_9\text{O}_{15}$. *Ceram. Int.* **47**, 5341–5346 (2021)
 17. Y. Slimani, N.A. Algarou, M.A. Almessiere, A. Sadaqat, M.G. Vakhitov, D.S. Klygach, D.I. Tishkevich, A.V. Trukhanov, S. Güner, A.S. Hakeem, I.A. Auwal, A. Baykal, A. Manikandan, I. Ercan, Fabrication of exchanged coupled hard/soft magnetic nanocomposites: correlation between composition, magnetic, optical and microwave properties. *Arab. J. Chem.* **14**(3), 102992 (2021)
 18. N.A. Algarou, Y. Slimani, M.A. Almessiere, S. Güner, A. Baykal, I. Ercan, P. Kögerler, Exchange-coupling effect in hard/soft $\text{SrTb}_{0.01}\text{Tm}_{0.01}\text{Fe}_{11.98}\text{O}_{19}/\text{AFe}_2\text{O}_4$ (where $\text{A}=\text{Co}, \text{Ni}, \text{Zn}, \text{Cu}$ and Mn) composites. *Ceram. Int.* **46**, 7089–7098 (2020)
 19. N.A. Algarou, Y. Slimani, F.S. Alahmari, M.G. Vakhitov, D.S. Klygach, S.V. Trukhanov, A.V. Trukhanov, A. Baykal, Magnetic and microwave properties of $\text{SrFe}_{12}\text{O}_{19}/\text{M}\text{Ce}_{0.04}\text{Fe}_{1.96}\text{O}_4$ ($\text{M} = \text{Cu}, \text{Ni}, \text{Mn}, \text{Co}$ and Zn) hard/soft nanocomposites. *J. Mater. Res. Technol.* **9**(3), 5858–5870 (2020)
 20. H. Khanduri, M. Chandra Dimri, H. Kooskora, I. Heinmaa, G. Viola, H. Ning, M.J. Reece, J. Krustok, R. Stern, Structural, dielectric, magnetic, and nuclear magnetic resonance studies of multiferroic Y-type hexaferrites. *J. Appl. Phys.* **112**, 073903 (2012)
 21. A.V. Trukhanov, V.G. Kostishyn, L.V. Panina, V.V. Korovushkin, V.A. Turchenko, P. Thakur et al., Control of electromagnetic properties in substituted M-type hexagonal ferrites. *J. Alloys Compd.* **754**, 247–256 (2018)
 22. N. Rezlescu, C. Doroftei, E. Rezlescu, P.D. Popa, The influence of heat-treatment on microstructure and magnetic properties of rare-earth substituted $\text{SrFe}_{12}\text{O}_{19}$. *J. Alloys Compd.* **451**, 492–496 (2008)
 23. N. Rezlescu, E. Rezlescu, C. Pasnicu, M.L. Craus, Improvement of the magnetic properties for Mn–Ni–Zn ferrites by rare earth Nd^{3+} ion substitution. *J. Phys.* **6**, 5707–5716 (1994)
 24. L.F. Chen, C.K. Ong, C.P. Neo, V.V. Varadan, V.K. Varadan, *Microwave Electronics: Measurement and Materials Characterization* (Wiley, Hoboken, 2004)
 25. B. Unal, M.A. Almessiere, Y. Slimani, A. Baykal, A.V. Trukhanov, I. Ercan, The conductivity and dielectric properties of neobium substituted Sr–NHF. *Nanomaterials* **9**, 1168 (2019)
 26. N.A. Algarou, Y. Slimani, M.A. Almessiere, S. Rehman, M. Younas, B. Unal, A. Demir Korkmaz, M.A. Gondal, A.V. Trukhanov, A. Baykal, I. Nahvi, Developing the magnetic, dielectric and anticandidal characteristics of $\text{SrFe}_{12}\text{O}_{19}/x(\text{Mg}_{0.5}\text{Cd}_{0.5}\text{Dy}_{0.03}\text{Fe}_{1.97}\text{O}_4)$ hard/soft ferrite nanocomposites. *J. Taiwan Inst. Chem. Eng.* **113**, 344–362 (2020)
 27. P. Piekarz, K. Parlinski, A.J.M. Oleś, Mechanism of the verwey transition in magnetite. *Phys. Rev. Lett.* **97**, 156402 (2006)
 28. Y. Slimani, B. Unal, M.A. Almessiere, A. DemirKorkmaz, A. Baykal, Investigation of AC susceptibility, dielectric, and electrical properties of Tb–Tm co-substituted M-type Sr hexaferrites. *Mater. Chem. Phys.* **260**, 124162 (2021)
 29. T. Honegger, K. Berton, E. Picard, D. Peyrade, Determination of Clausius–Mossotti factors and surface capacitances for colloidal particles. *Appl. Phys. Lett.* **98**, 181906 (2011)
 30. C.G. Koops, On the dispersion of resistivity and dielectric constant of some semiconductors at audio frequencies. *Phys. Rev.* **83**, 121–124 (1951)
- Publisher's Note** Springer Nature remains neutral with regard to jurisdictional claims in published maps and institutional affiliations.